A hierarchical modeling approach to the simulation and control of planar solid oxide fuel cells

Marco Sorrentino [a,*], Cesare Pianese [a], Yann G. Guezennec [b]

[a] *Department of Mechanical Engineering, University of Salerno, Via Ponte Don Melillo, 84084 Fisciano (SA), Italy*
[b] *Department of Mechanical Engineering, The Ohio State University, Columbus, OH 43210, USA*

Abstract

The main aim of the paper is to propose hierarchical modeling as a suitable methodology to perform control-oriented analysis of planar solid oxide fuel cells (P-SOFC).

At the high level of the hierarchical structure is a one-dimensional, steady-state model, developed referring to the state of the art in the field of SOFC modeling. Validation is conducted via comparison with both experimental tests and standard references derived from literature.

In the proposed modeling structure, at the low-level is the control-oriented model, developed on the basis of the information provided by the higher level model and assuming the SOFC behaves as a first-order system. The thermal dynamics is considered dominant with respect to both electrochemistry and mass transfer dynamics. Therefore, SOFC transients are modeled applying the conservation of energy principle (heat balance) to a lumped control volume, including interconnect, electrolyte and electrodes. Due to the lack of suitable experimental data, model accuracy is verified by comparing the simulated fuel cell response to similar data available in literature, generated by means of a physical comprehensive model.

Extensive simulations of the fuel cell dynamic behavior are performed to analyze in detail the SOFC dynamics with respect to load changes. Furthermore, an application example is given, dealing with the development of a PI controller to limit temperature rise across the cell within a safe range.

1. Introduction

Nowadays the development of clean energy systems, for both transportation and stationary applications, is recognized as mandatory to satisfy well-known environmental and regulatory requirements in terms of emissions and energy conversion efficiencies. Because of their high efficiencies and zero toxic emission levels (only the CO_2 released by the hydrogen production process is a concern) fuel cell systems are considered as one of the most attractive solution by the automotive and power generation industry, and by many research/academic organizations.

Among the existing fuel cell technologies, solid oxide fuel cells are particularly suitable for both stationary and mobile applications, due to their high energy conversion efficiency, modularity, low emissions and noise and high fuel flexibility [1,2]. Moreover, the high working temperatures (up to 1000 °C) suggest their use in highly efficient cogeneration applications. SOFCs also offer the opportunity of internally reforming the fuel (e.g. natural gas, propane, methanol, gasoline, diesel, etc.), making it possible to avoid using highly sophisticated, expensive external reformer [2] and simplify fuel storage [1]. Nevertheless, the big challenges to promote SOFC systems diffusion are related to the increase in fuel cell lifetime and decrease in production cost. These issues have been substantially addressed by the Solid state Energy Conversion Alliance (SECA), a platform involving relevant partners such as the US Department Of Energy (DOE) and Siemens Westinghouse, which are among others the leading institutions in SOFC research. Specifically, they jointly defined [1] a 10 years program (2002–2012), claiming the need of concentrating the research efforts towards the development of a low-cost (e.g. 400 $ kW^{-1}) 10 kW SOFC mod-

* Corresponding author. Tel.: +39 089964080; fax: +39 089964037.
E-mail address: msorrentino@unisa.it (M. Sorrentino).

Nomenclature

A	electroactive area (cm^2)
$\dot{E}$	energy rate (W)
$\dot{E}_{el}$	electric power (W)
E_{Nernst}	Nernst potential (V)
F	Faraday constant ($A\,s\,mol^{-1}$)
G	Gibbs free energy ($J\,mol^{-1}$)
I_{SOFC}	total operating current (A)
J	current density ($A\,cm^{-2}$)
$\bar{J}$	average current density ($A\,cm^{-2}$)
l	thickness (cm)
$\dot{n}_j$	molar flow for specie j ($mol\,s^{-1}$)
N	number of computational elements
p_{CH_4}	methane partial pressure (bar)
p_{H_2}	hydrogen partial pressure (bar)
p_{H_2O}	water partial pressure (bar)
p_{O_2}	oxygen partial pressure (bar)
$\dot{Q}_{conv}$	convective heat transfer (J s)
R	universal gas constant ($J\,mol^{-1}\,K^{-1}$)
t	time (s)
T	temperature (K)
T_{out}	outlet temperature (K)
U_f	fuel utilization
V_{act}	activation polarization (V)
V_{conc}	concentration polarization (V)
V_{offset}	voltage offset (V)
V_{Ohm}	Ohmic polarization (V)
V_{SOFC}	SOFC voltage (V)
$V_{v,an}, V_{v,ca}$	electrodes porosity
x_j	molar fraction for the j-th specie

Greek letters

Δ	change
λ	excess of air fed to the SOFC
σ	ionic/electronic conductivity ($S\,cm^{-1}$)

Superscripts

i	i-th computational element
pre	pre-reformer input
0	boundary conditions (i.e. cell inlet)

Subscripts

a	air gas
an	anode
ca	cathode
eff	effective
el	electrolyte
f	fuel gas
in	SOFC inlet
min	minimum
out	SOFC outlet
ox	oxidation reaction
prod	product
react	reacted/reactant
s	solid trilayer (i.e. electrolyte and electrodes)
∞	final stationary point in step change
0	initial stationary point in step change

ule, flexible enough to be applied in transportation, auxiliary power units (APUs) and stationary power plants. The achievement of such an objective will surely contribute to promoting the technology and finally starting a mass production phase. Once this goal is reached, potential areas of application in the short term will be small residential power generators and vehicles' APUs. In the long-term scenario, SOFC applications could be reasonably extended to marine and rail APUs, to high-power stationary generators and even to marine and rail propulsion [3,4].

According to SECA program, the short-term implementation of SOFC can be pursued by addressing the following highly sensitive points [1]:

1. Operating temperature reduction;
2. Definition of optimal cell configuration;
3. Optimal balance of plant;
4. Use of liquid fuels.

SOFC operating features and the success achieved by some prototypal applications [5] lead to consider point 4 not as troublesome as points 1–3, for which considerable efforts have to be made by the researchers active in this field. Particularly, letting SOFC work at lower temperatures would surely enhance technological feasibility, with the draw back of lowering efficiency too. Thus, the optimal temperature range has to be found as the best trade-off between material specifications and efficiency [2]. Moreover, cell design has to be chosen in such a way to maximize system efficiencies and reduce the risk of components damage. Planar designs have lower electrical resistance than tubular, thus guaranteeing higher energy conversion efficiency and, in turn, higher specific power (i.e. up to $1.2\,W\,cm^{-2}$) [2]. Regarding gas-feeding, co-flow ensures a more even temperature distribution in the flow direction as compared to counter-flow, which is instead characterized by dangerous thermal mismatches with respect to components integrity [6]. Thus, choosing a planar co-flow configuration positively impacts production cost and technological feasibility.

Optimal system design and components sizing, both strategic activities with respect to SECA goals, require computational tools that meet the conflicting needs of accuracy, affordable computational time, limited experimental efforts and flexibility. In this context, hierarchical modeling of SOFC systems represents a very suitable methodology to enhance both design and sizing phases, with the final aim of moving from a developmental stage to a mass production phase [8,9]. The potentialities of hier-
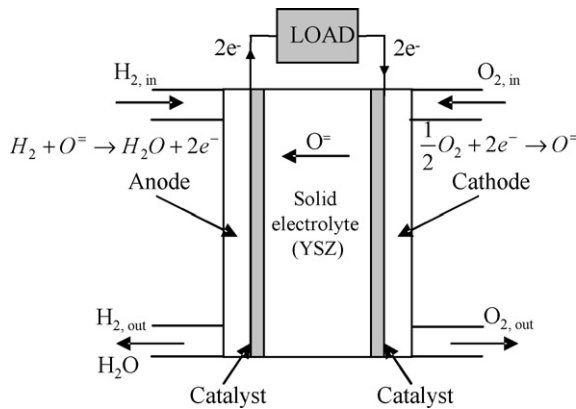
Fig. 1. Schematic of SOFC working principle.

archical modeling were already analyzed and proven to be very effective in other research fields, such as automotive engines control. Arsie et al. [7] discussed how only the use of black-box and gray-box engine models seems compatible with the high number of function evaluation required to determine optimal control strategies. Nevertheless, such a choice requires a relevant number of experimental data for model validation, due to the lack of built-in physical information. Therefore, more informative thermodynamic models, which would require a more limited number of experimental data to be validated, could be used off-line to perform virtual engine testing aiming at extending the available data-set. Such an extended data-set, following the hierarchical approach, can in turn be exploited to enhance black-box models identification and validation.

This work focuses on modeling SOFC in both stationary and transient conditions. Particularly, the aspects related to SOFC dynamic behavior and control were deeply analyzed, as a consequence of the up-to now limited literature on these topics. The next sections present in detail the hierarchical approach that has been proposed to develop a control-oriented model of a single planar co-flow SOFC fed with reformate fuel.

2. Solid oxide fuel cells

2.1. Working principle

Fig. 1 describes the basic working principle of an SOFC. For sake of clearness, in the figure only the electro-oxidation reaction is described, while methane reforming and related water–gas-shift are not included. A single cell consists of three main components: an anode, a cathode and a solid electrolyte separating the two electrodes. Air and hydrogen (i.e. the reactants) flow through cathode and anode, respectively. Under electrical load, at the cathode surface the presence of perovskite catalyst enables oxygen ionization. The solid electrolyte permits the flux of oxygen ions to the anode, where they electro-oxidize hydrogen, thus releasing heat, water and electrons. Since electrolyte material ensures quasi-zero electronic conductivity, electrons are forced to flow through interconnect and external load towards the cathode, thus closing the electrical loop.

2.2. Application of SOFC in hybrid auxiliary power units

As a consequence of their high fuel flexibility, many researchers are considering the use of SOFCs for transportation application, especially to face well known issues associated with on-board storage of H_2. Particularly, as outlined by SECA [1], SOFCs are currently being preferred with respect to PEM fuel cells for automotive auxiliary power units. This happens despite the slow start-up and besides the fuel flexibility, because of the following benefits: cogeneration and internal reforming opportunities; no need of water management; simple reformer technology; high electrical efficiency; no noble catalysts; low noise [5,8]. Therefore, many prototypal applications of automotive APUs are available in literature. Among them, the one jointly developed by BMW and Delphi [5] can be rightly considered as the most relevant.

SOFC-APUs are usually assembled into a hybrid configuration, in which the fuel cell stack interacts with the auxiliary components to match the load request. A simple schematic of a reformate-fed automotive APU is given in Fig. 2, where a considerable number of devices to assist stack operation is required. An air-blower (or a compressor in case of pressurized cells) feeds air to the stack. Post-burner and heat exchangers recover energy from the exhaust gases to warm-up the incoming air flow and to yield thermal power on output, which is usually in the ratio of 1 to 1.5 with the electric power [10]. A fuel reformer processes methane (or other hydrogen-rich fuels) using the heat recovered from the exhausts. A battery pack supports the stack in supplying electrical energy during system warm-up and peak-power phases; moreover, it allows for energy storage during low-power phases. Power conditioning devices are needed to convert dc into ac and boost the voltage.

The prototype developed by Delphi and BMW showed the benefits achievable with regard to on-board independent electrification. Nevertheless, the success of this technology in the automotive field strongly depends on the solution of limiting factors such as slow dynamics, thermal-stress-related issues and low power to weight ratio (i.e. $0.1\,kW\,kg^{-1}$) [8]. Therefore,
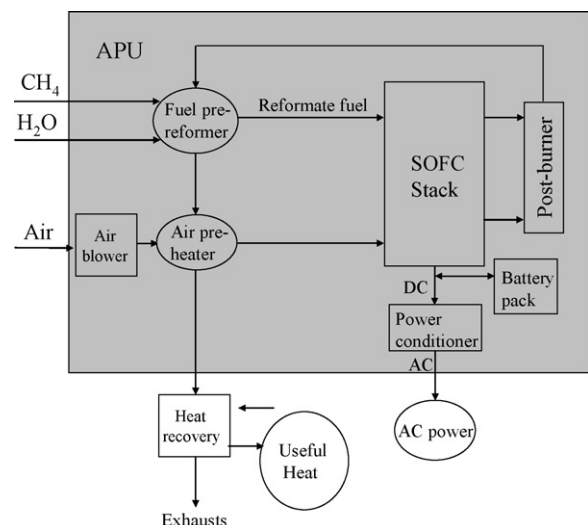

Fig. 2. Block diagram of a typical reformate-fed APU with energy flow paths.

automotive SOFC-APUs require precise design of the system (i.e. balance of plant) together with the definition of the optimal energy-management strategies. This can be accomplished by developing advanced simulation procedures with a satisfactory compromise between prediction accuracy and computational burden.

Potential automotive applications of the APU module shown in Fig. 2 include [11]:

- *Mild hybrids*: SOFC supplies electric and thermal energy for hotel functions when the engine (ICE) is turned off.
- *Full hybrid*: SOFC supports ICE in powering the vehicle, allows to reduce battery size and replaces the engine in urban driving.
- *EV range extender*: SOFC recharges battery during trip to extend battery autonomy. SOFC is operated steadily at its maximum efficiency depending on driving conditions.

At the end of this general overview on automotive SOFC APUs applications, it is worth mentioning that the experience gained through automotive APU development could be reasonably re-scaled and then extended to rail and marine propulsion, where power demands are less fluctuating than automotive ones.

3. Hierarchical approach to SOFC-APU modeling and control

The recourse to a hierarchical modeling approach is motivated by the high computational intensity characterizing optimization algorithms, especially those aiming at large scale system design (e.g. automotive propulsion systems) [12]. In principle, this issue may be satisfactorily addressed by exclusively using black-box/lumped models of the system under development. Nevertheless, against such choice are major drawbacks, such as the very extended data-sets required for identification and validation of black-box models, together with the need of running new experiments whenever system specifications change.

Arsie et al. [13] demonstrated, with regard to internal combustion engine modeling, that the best compromise between precision, experimental costs, computational time and flexibility is achieved by using a mixed modeling approach, with phenomenological, gray- and black-box models integrated within a hierarchical structure. This approach can be usefully extended to SOFC automotive APUs, especially because of the high costs to be faced to run transient experiments and the high variety of fuel cell designs currently under-investigation.

The hierarchical approach adopted in the present work is sketched in Fig. 3. The levels (a)–(c) are representative of the different physical contents. At the highest level (i.e. (a)) is the real system. For the purposes of the present work, an anode-supported SOFC experimented by the Pacific Northwest National Laboratory was chosen [14]. The corresponding polarization curves were used to develop a one-dimensional (1D) steady-state model (i.e. task 1, detailed in Section 4), which is placed at level (b). Thanks to its sufficiently high physical content, such model is suitable to simulate planar co-flow SOFCs
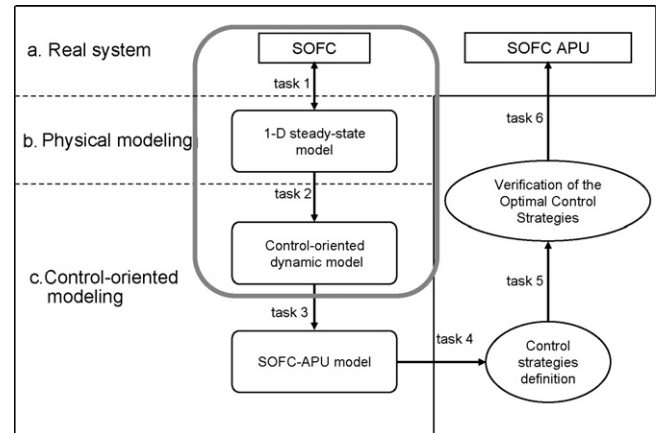

Fig. 3. Hierarchical approach for modeling (tasks 1 and 2), simulation (task 3), control strategies definition (tasks 4 and 5) and implementation (task 6) of an SOFC-APU. The gray smooth-cornered box highlights the tasks accomplished in this paper.

for both anode- and electrolyte-supported cell. Moreover, both pure H_2 and reformate fuel feeds can be considered.

Standing the dominance of thermal dynamics in SOFC transient behavior, gas mass transfer and electrochemistry dynamics can be safely neglected [15]. Therefore, temperature and voltage dynamics were modeled applying the first principle of Thermodynamics to a lumped cell unit. The physical model (i.e. one-dimensional) was used to extend the reference data-sets, with the final aim of identifying a suited black-box relationship for SOFC voltage estimation. Such relationship was embedded in the dynamic equation, yielding a control-oriented model for simulation of planar co-flow SOFCs (i.e. task 2, detailed in Section 5). Such model, due to its low physical content, is placed at the bottom level (i.e. (c)) of the hierarchical structure described in Fig. 3.

Fig. 3 also covers the on-going and future activities that will follow the present work. Task 3 will focus on the development of a comprehensive model of an automotive SOFC-APU, as the one shown in Fig. 2. Afterwards, through task 5 the supervisory and low-level control strategies, to be developed via model-based approaches (i.e. task 4), are intended to be validated on a real system. The final objective (i.e. task 6) will aim at providing useful methodologies and tools for improving both design and control of automotive APUs.

4. One-dimensional steady-state modeling of planar SOFC

The one-dimensional modeling of co-flow planar SOFC (see Fig. 3) allows achieving a satisfactory compromise between the conflicting needs of high model precision and affordable computational burden. The knowledge of the spatial distributions of current, temperature and partial pressures in the flow direction allows for accurate prediction of cell performance. On the other hand, avoiding to solve the governing equations in the other dimensions results in significant reduction of computational time. Therefore, the recourse to a 1D model is particularly promising for SOFC-related optimization problems, such as

balance of plant analyses and polarization models identification. Moreover, the high physical content guaranteed by a 1D approach provides considerable flexibility to account for different cell geometries, materials and fuel feeds (fully or partially reformed petroleum fuels). The above features are particularly useful to perform "virtual experiments" throughout the SOFC operating domain. This serves at the central aim of the research, which is the development of black-box models via hierarchical approach for real-time and control applications.

Modeling electrochemistry and mass transfer inside the fuel cell entails simultaneously solving the equations of energy, mass, and voltage conservation. The developed model consists of a set of sub-models, namely energy, material and electrochemical balance, that are executed in an iterative procedure in the Matlab© environment. The model accounts for variations in the cell by discretizing the domain into computational elements along the cell length. The computation starts at the inlet section of the fuel/air flows and marches forward in the streamwise direction [10,16]. At each computational element, balances for mass, energy and electric potential are applied in order to derive a closed form. The cell is assumed to be isopotential [10] and fully stirred conditions are considered at the element level. Assuming uniform distribution but no mixing of air and fuel feed gases, the two streams are treated separately as perfect gases. Pressure drop across the fuel and air channels is neglected according to the indications provided in [17]. Additional assumptions for each of the sub-models are presented later on.

4.1. Electrochemical model

The electrochemical sub-model evaluates SOFC voltage and power along the flow direction. The computational domain is sketched in Fig. 5. For each element i the current density is calculated by Faraday's law:

$$J^i = \frac{\dot{r}^i_{ox} F n_e}{A^i} \qquad (1)$$

where n_e is the number of electrons transferred per molecule of H_2 (i.e. $n_e = 2$), $\dot{r}^i_{ox}$ is the reaction rate (mol s^{-1}) of the electro-oxidation reaction and A^i (cm^2) is the area of the single computational element (i.e. $A^i = A/N$). Multiplying the current density of each element by A^i, the total current is found summing up the contributions from the N computational elements:

$$I_{SOFC} = \sum_{i=1}^{N} (J^i A^i) \qquad (2)$$

The ideal potential difference between anode and cathode is evaluated using the Nernst equation:

$$E^i_{Nernst} = -\frac{\Delta G^i_{ox}(T^i_s)}{n_e F} - \frac{R T^i_s}{n_e F} \ln \left(\frac{p^i_{H_2O}}{p^i_{H_2} \sqrt{p^i_{O_2}}} \right) \qquad (3)$$

There are three major forms of polarization losses: activation, Ohmic and concentration. A minor constant offset also contributes to the total polarization, which is the result of minor losses such as contact resistance, internal current and leaks. Following [18], the offset was assumed equal to 0.07 V. The sum of the different polarizations results in the voltage drop from ideal Nernst potential to effective operating value. Since interconnect and electrodes are isopotential, cell voltage is constant over the whole cell and can be estimated as

$$V_{SOFC} = E^i_{Nernst} - V^i_{Act} - V^i_{Ohm} - V^i_{Conc} - V_{Offset} \qquad (4)$$

The total power drawn from the SOFC is calculated as

$$\dot{E}_{el} = V_{SOFC} I_{SOFC} \qquad (5)$$

where I_{SOFC} is given by Eq. (2). The following three sections treat in detail modeling of activation, Ohmic and concentration polarization. It is worth remarking that model parameters were identified versus the polarization curves provided in [14], which were measured on an anode-supported SOFC operated at constant temperature and fed with pure H_2. Particularly, the parameters were identified against the voltage values corresponding to 0.5 A cm^2, with cell temperature ranging from 650 to 800 °C. Thus, with only four measurements it was possible to identify a reliable polarization model, as confirmed by the comparison between experiments and model outputs over a wide operating domain, as shown in Fig. 4. The next sub-sections provide the theoretical basis of polarization losses estimation. For further details on this identification task and the resulting parameters value, the reader is addressed to a previous work [19].

4.1.1. Activation polarization

Activation polarization represents the energy barrier to be overcome to activate the electrochemical reactions occurring at the electrodes surface [20]. This amount of energy inevitably causes a significant voltage loss, which is usually modeled through the non-linear relationship known as Butler–Volmer equation [21]:

$$V^i_{Act} = \frac{R T^i_s}{\alpha(T^i_s) F} \sinh^{-1} \left(\frac{J^i}{2 J_0(T^i_s)} \right) \qquad (6)$$
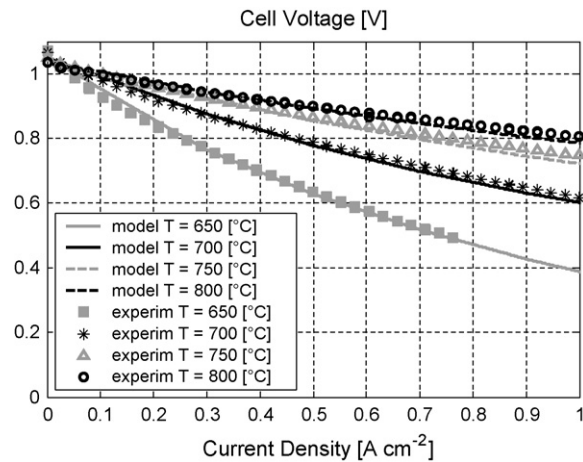

Fig. 4. Comparison between experiments and model outputs for the anode-supported SOFC used as reference to identify the electrochemical model parameters.

where α is the charge transfer coefficient and J_0 is the exchange current density.

4.1.2. Ohmic polarization

Ohmic polarization mainly depends on the electronic conductivity of electrodes and the ionic conductivity of the electrolyte. Such losses are estimated summing up the contribution from each SOFC part (i.e. anode, cathode and electrolyte), as follows:

$$V_{\text{ohm},k}^i = \frac{l_k}{\sigma_k(T_s^i)} J^i$$
$$V_{\text{ohm}}^i = \sum_k V_{\text{ohm},k}^i \quad k = [\text{an, ca, el}] \tag{7}$$

Conductivities are estimated by means of correlations, proposed in literature [18] for second-generation ceramic SOFC, in which the materials of anode, cathode and electrolyte are, respectively, nickel-cermets, strontium-doped lanthanum manganite and yttria-stabilized zirconia:

$$\sigma_{\text{an}} = 1000 \tag{8}$$

$$\sigma_{\text{ca}}(T_s) = C_1(T_s^i)^2 - C_2 T_s^i + C_3 \tag{9}$$

$$\sigma_{\text{el}}(T_s) = C_4(T_s^i - 273)^2 + C_5(T_s^i - 273) + C_6 \tag{10}$$

The effect of electrodes porosity is taken into account by correcting anode and cathode conductivity as follows:

$$\sigma_{\text{an,eff}} = \sigma_{\text{an}}(1 - 1.8 V_{v,\text{an}}) \tag{11}$$

$$\sigma_{\text{ca,eff}} = \sigma_{\text{ca}}(1 - 1.8 V_{v,\text{ca}}) \tag{12}$$

4.1.3. Concentration polarization

As fuel is depleted, hydrogen and oxygen partial pressures decrease at anode and cathode, respectively. The depletion rate depends on average current density drawn from the cell. As the current density increases, the partial pressures decrease and eventually an insufficient amount of reactants are transported to the electrodes. This results in significant losses until the voltage is reduced to 0 [22,23]. The values at which such phenomenon occurs are known as anode and cathode limiting currents. This voltage loss, which is dominant at high current densities, is called concentration polarization and can be estimated as follows:

$$V_{\text{Conc}}^i = -\frac{RT_s^i}{2F} \left[\frac{1}{2} \ln\left(1 - \frac{J^i}{J_{cs}}\right) + \ln\left(1 - \frac{J^i}{J_{as}}\right) \right.$$
$$\left. - \ln\left(1 + \frac{p_{\text{H}_2}^i J^i}{p_{\text{H}_2\text{O}}^i J_{as}}\right) \right] \tag{13}$$

The anode and cathode limiting currents (i.e. J_{as} and J_{cs}, respectively) are computed as function of species diffusion coefficients, following the approach proposed in [10].

4.2. Conservation equations

Conservation of mass, energy and electric potential are applied to each computational element in the flow direction. Momentum equation was not considered since it is assumed that
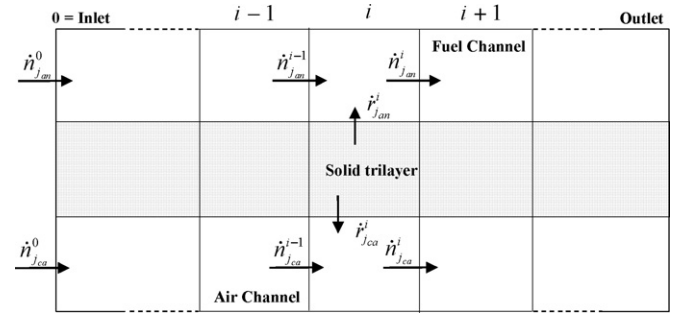

Fig. 5. Discretized mass balance at the i-th element.

pressure drop across the cell can be neglected. The structure of models was conceived in such a way to account for internal reforming of a partially pre-reformed methane feed.

4.2.1. Electric potential balance

Since the interconnect and the electrodes are assumed to be isopotential, the voltage is constant over the whole cell, thus yielding the following balance to be solved for each computational element:

$$E_{\text{Nernst}}^i - V_{\text{Act}}^i - V_{\text{Ohm}}^i - V_{\text{Conc}}^i - V_{\text{Offset}} - V_{\text{SOFC}} = 0 \tag{14}$$

4.2.2. Material balance

Anode and cathode are discretized in the flow direction as shown in Fig. 5, where inlet, outlet and source (or sink) molar flows are represented for the i-th element and the j_{an}-th and j_{ca}-th specie. Applying conservation of mass principle to the discretized cell for all the species, the following material balances result:

$$\text{anode}: \begin{cases} \dot{n}_{\text{H}_2}^i = \dot{n}_{\text{H}_2}^{i-1} + 3\dot{r}_{\text{ref}}^i + \dot{r}_{\text{shift}}^i - \dot{r}_{\text{ox}}^i \\ \dot{n}_{\text{CH}_4}^i = \dot{n}_{\text{CH}_4}^{i-1} - \dot{r}_{\text{ref}}^i \\ \dot{n}_{\text{H}_2\text{O}}^i = \dot{n}_{\text{H}_2\text{O}}^{i-1} - \dot{r}_{\text{ref}}^i - \dot{r}_{\text{shift}}^i + \dot{r}_{\text{ox}}^i \\ \dot{n}_{\text{CO}}^i = \dot{n}_{\text{CO}}^{i-1} + \dot{r}_{\text{ref}}^i - \dot{r}_{\text{shift}}^i \\ \dot{n}_{\text{CO}_2}^i = \dot{n}_{\text{CO}_2}^{i-1} + \dot{r}_{\text{shift}}^i \end{cases} \tag{15}$$

$$\text{cathode}: \dot{n}_{\text{O}_2}^i = \dot{n}_{\text{O}_2}^{i-1} - 0.5\dot{r}_{\text{ox}}^i \tag{16}$$

The quantities $\dot{r}_{\text{ref}}^i$, $\dot{r}_{\text{shift}}^i$ and $\dot{r}_{\text{ox}}^i$ in Eqs. (15) and (16) represent, respectively, the reaction rates (mol s^{-1}) of the methane reforming (Eq. (17)), water–gas shift (Eq. (18)) and electro-oxidation (Eq. (19)) reactions, reported below:

$$\text{CH}_4 + \text{H}_2\text{O} \rightarrow \text{CO} + 3\text{H}_2 \tag{17}$$

$$\text{CO} + \text{H}_2\text{O} \leftrightarrow \text{CO}_2 + \text{H}_2 \tag{18}$$

$$\text{H}_2 + \frac{1}{2}\text{O}_2 \rightarrow \text{H}_2\text{O} \tag{19}$$

$\dot{r}_{\text{ox}}^i$ and $\dot{r}_{\text{ref}}^i$ are estimated, respectively, via Faraday's law (Eq. (1)) and the following temperature–pressure-dependent correlation proposed by Achenbach and Riensche [24]:

$$\dot{r}_{\text{ref}}^i = 4274 p^i A^i e^{-(82000/R/T_f^i)} \tag{20}$$

On the other hand, since the water–gas-shift reaction is assumed to be at equilibrium, $\dot{r}_{shift}^i$ is estimated solving the equilibrium constant with respect to species molar fraction [19,25].

Boundary conditions for the systems of Eqs. (15) and (16) are the inlet flows, estimated according to the operating fuel utilization and excess air factors:

$$U_f = \frac{\dot{n}_{H_2,react}}{4\dot{n}_{CH_4}^{pre}} = \frac{I_{SOFC}}{Fn_e}\frac{1}{4\dot{n}_{CH_4}^{pre}} \quad (21)$$

$$\lambda = \frac{\dot{n}_{O_2}^0}{\dot{n}_{O_2,sto}} = \frac{\dot{n}_{O_2}^0}{(1/2)\dot{n}_{H_2,react}} = \frac{\dot{n}_{air}^0}{4.76(1/2)\dot{n}_{H_2,react}} \quad (22)$$

4.2.3. Energy balance

The energy balance is verified by dividing the computational element into three separate control volumes, namely solid trilayer and fuel and air channels (see Fig. 6). The following simplifying hypotheses were assumed: (i) adiabatic cell boundaries; (ii) radiative heat transfer between solid trilayer and metallic interconnects is negligible; (iii) conduction in the solid trilayer in the flow direction is neglected. Hypothesis (i) is consistent with the assumptions suggested in [10]. Hypothesis (ii) was verified by comparing model outputs with corresponding data provided by the International Energy Agency (IEA) [10] (see Table 2). The last assumption (iii) also was confirmed by the results presented in [17]. Hence, the dominant processes described in the model are the convective heat transfer between solid trilayer and fuel and air streams, and the energy transfer due to the reactants and products flows.

Applying energy conservation principle to the three control volumes shown in Fig. 6, the following energy balances hold for solid trilayer, fuel channel and air channel, respectively:

$$\dot{E}_{react}^i - \dot{E}_{prod}^i + \dot{E}_{O_2}^i - \dot{Q}_{conv,s-f}^i - \dot{Q}_{conv,s-a}^i - \dot{E}_{el}^i$$
$$= 0 \quad (solid) \quad (23)$$

$$\dot{E}_f^{i-1} - \dot{E}_f^i - \dot{E}_{react}^i + \dot{E}_{prod}^i + \dot{Q}_{conv,s-f}^i = 0 \quad (fuel) \quad (24)$$

$$\dot{E}_a^{i-1} - \dot{E}_a^i - \dot{E}_{O_2}^i + \dot{Q}_{conv,s-a}^i = 0 \quad (air) \quad (25)$$

Further details on the estimation of the energy rates, associated with inlet and outlet flows and the electro-oxidation, reforming and water–gas-shift reactions, can be found in [19].
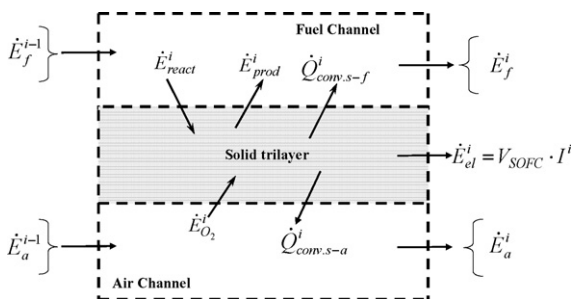

Fig. 6. Energy balance at the *i*-th element.

Table 1
Specifications of the electrolyte-supported SOFC defined by IEA [10]

Geometrical data	
Electroactive area	100 cm^2
Cell length	10 cm
Channel width	3 mm
Channel height	1 mm
Anode thickness	50 μm
Cathode thickness	50 μm
Electrolyte thickness	150 μm
Bipolar plates thickness	2500 μm
Operating conditions	
Pressure	1 bar
Inlet temperature	900 °C
Fuel utilization	85%
Excess air	7
Average current density	0.3 A cm^{-2}

Fuel feed	Reformate methane
Inlet fuel composition	17.1% CH$_4$; 26.26% H$_2$; 49.34% H$_2$O; 2.94% CO; 4.36% CO$_2$
Inlet air composition	21% O$_2$; 79% N$_2$

4.3. Model validation

Provided that the fuel cell is discretized on an N computational elements grid, the one-dimensional model results in a system of $10N+1$ equations (i.e. Eqs. (14)–(16) and (23)–(25) plus the constraint, expressed by Eq. (2), on total current drawn from the fuel cell). The $10N+1$ unknowns are

$$\left\{J^i, T_a^i, T_f^i, T_s^i, x_{H_2}^i, x_{CO}^i, x_{CO_2}^i, x_{CH_4}^i, x_{H_2O}^i, x_{O_2}^i, V_{SOFC}\right\} \quad (26)$$

The model was tested by estimating the spatial distributions of J and T_s and than comparing some suitable metrics with published data. The specifications of the reference planar SOFC are given in Table 1, which also reports the operating conditions at which the one-dimensional model was solved.

Figs. 7 and 8 show the spatial distributions of current, temperature and fuel-species molar fraction. Initially, current density follows temperature variation, which decreases significantly (from 900 down to 850 °C) due to the highly endothermic inter-
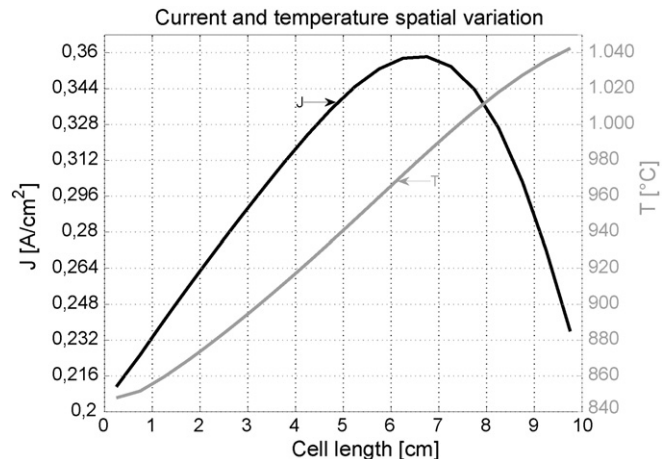

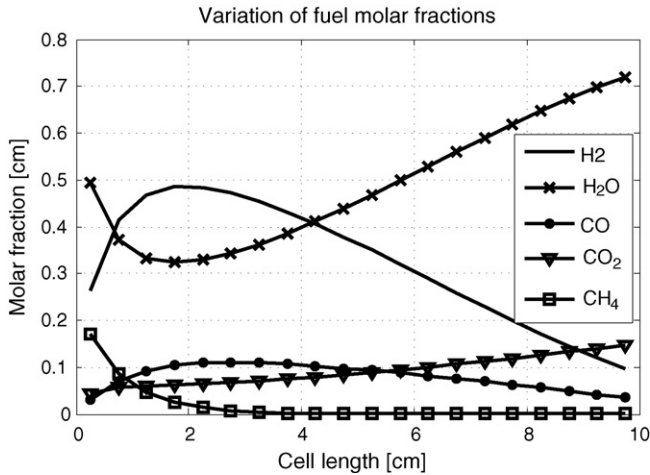Fig. 7. Estimated current and temperature distributions for the IEA SOFC.

Fig. 8. Estimated fuel gas composition for the IEA SOFC.

nal reforming of methane. Then, after the methane is completely reformed (i.e. at one-fourth of cell length, as shown in Fig. 8), temperature and hydrogen molar fractions increase, with a beneficial impact on polarization losses (see cell temperature effect in Fig. 4) and Nernst potential (see impact of hydrogen partial pressure in Eq. (2)), respectively. Therefore, the electrochemical reactions are enhanced, causing current to reach its maximum value (beyond 7 cm in Fig. 7). Finally, due to hydrogen depletion as shown in Fig. 8, current decreases monotonically.

As shown in Table 2, the comparison between calculated and published outputs confirms the good level of accuracy achieved and the validity of model assumptions.

5. Control-oriented model for simulation and control of planar SOFC

The control-oriented model is based on simplifying assumptions whose validity is supported by previous studies. Such assumptions, presented in detail in the next sections, allow describing the dynamic behavior of a single SOFC as a first order system with the outlet temperature as the only state variable. This simplification entailed developing a black-box relationship between V_{SOFC}, state variable (i.e. T_{out}) and input variables (i.e. $\bar{J}$, and λ). The data needed for identifying this relationship were generated making use of the high-level model (i.e. the 1D model described in Section 4) of the hierarchical structure shown in Fig. 3. The hierarchical approach was followed to derive the voltage model for a reformate-fuel-fed SOFC, considering the cell dimensions provided by IEA (see Table 1). The validity of the control-oriented model was checked by simulating load

Table 2
Comparison between model and IEA data published in [10]

	IEA	Model
Max J(X) (A cm^{-2})	0.3040–0.3665	0.3582
Min J(X) (A cm^{-2})	0.1748–0.2508	0.2112
Max T(X) (°C)	1021–1034	1043
Min T(X) (°C)	847–862	848
Voltage (V)	0.633–0.649	0.649
Power (W)	18.99–19.47	19.47

steps and comparing the resulting voltage and outlet temperature responses with those obtained by a physical model [15]. Assuming the single SOFC as representative of the whole stack behavior, the extension of the developed model to an SOFC stack is straightforward.

5.1. Dynamic model

The dynamic, control-oriented model presented herein was conceived to describe the response of SOFC voltage to variations in load and excess air. Main goal was to develop a simplified model that guarantees a satisfactory trade-off between accuracy and computational burden. Therefore, SOFC dynamics is described via lumped modeling of the open system shown in Fig. 9. The model was obtained considering the following simplifying assumptions: (i) adiabatic cell (i.e. the heat exchange with the surroundings is zero) [10]; (ii) the variation of gases' sensible heat is neglected; (iii) negligible pressure drop across the cell [17]; (iv) the dynamics of both electrochemistry and mass transfer is much faster than thermal dynamics [15]; (v) since in planar co-flow SOFC fuel, air and solid temperatures do not differ significantly [26], the temperature of the solid trilayer is assumed as representative of the entire control volume; (vi) T_{out} is assumed as the state variable.

Starting from the above hypotheses, SOFC thermal dynamics can be modeled applying the energy conservation principle to the lumped volume shown in Fig. 9. Therefore, the following dynamic model was obtained:

$$K_{cell}\frac{dT_{out}}{dt} = \dot{E}_{in}(T_{in}) - \dot{E}_{out}(T_{out})$$
$$- \bar{J}V_{SOFC}(\bar{J}, T_{out}, \lambda)A \quad (27)$$

where K_{cell} (J K^{-1}) is the lumped heat capacity of the SOFC and $\dot{E}_{in}$ and $\dot{E}_{out}$ are the inlet and outlet energy flows, respectively. In Eq. (27), the accumulation term on the left hand side only accounts for the heat adsorbed by the solid part, as a consequence of hypothesis (ii).

Owing to the lumped nature of Eq. (27) and the simplifying modeling assumptions, it is required to identify the model parameter K_{cell}. Nevertheless, due to the lack of dynamic experimental data suitable for system identification [10], it was assumed that K_{cell} equals the heat capacity of the solid parts (i.e. cell trilayer and interconnect), as follows:

$$K_{cell} = \rho_{cer}VOLc_{cer} = 96.86 \, (J \, K^{-1}) \quad (28)$$
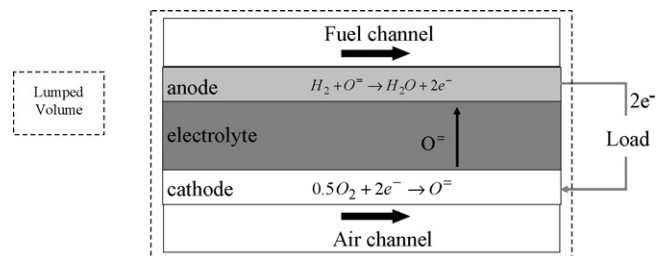

Fig. 9. Lumped cell that includes gas channels, solid trilayer and interconnect.

where VOL is the cell volume, calculated according to the geometrical data listed in Table 1, and ρ_{cer} (6600 kg m^{-3}) and c_{cer} (400 J kg^{-1} K^{-1}) are ceramic density and specific heat, respectively.

The state-space representation of Eq. (27) in its explicit form reads as

$$\begin{cases} \dot{x} = f(x, u) \\ y = g(x, u) \end{cases} \tag{29}$$

where the state, output and input vectors are, respectively:

$$x = \{T_{out}\} \qquad y = \{V_{SOFC}\} \qquad u = \{T_{in}, \bar{J}, \lambda\} \tag{30}$$

and $g(x,u) = g(\bar{J}, T_{out}, \lambda)$ is a black-box relationship presented in the next section.

The proposed model is characterized by two distinguishing features with respect to other lumped approaches proposed in literature [27]. Firstly, since the outlet temperature is the state variable, it is possible to account for temperature variation across the cell. Therefore, this model is suitable to perform, at low computational cost, very accurate balance of plant analyses, including heat exchangers sizing. Secondly, as a consequence of the hierarchical approach followed, the voltage is evaluated as function of the main operating variables (i.e. current density, outlet cell temperature and excess air), thus allowing to separately investigate the influence of each variable on SOFC performance in both steady and transient conditions.

5.2. SOFC voltage black-box model

According to the modeling scheme shown in Fig. 7, the relationship between cell voltage and state and input variables (i.e. $g(x,u)$) was hierarchically derived from the one-dimensional model developed in Section 4. Particularly, steady-state calculations performed on the IEA benchmark described in Table 1 were used to generate a reference data-set that comprehensively covers the SOFC operating domain. The reference data, used to identify and validate the voltage black-box model, were obtained setting the fuel utilization to 0.8 and varying the operating variables around their nominal values in the following ranges:

$$\bar{J} \, (\text{A cm}^{-2}) \in [0\text{–}0.8]; \quad T_{in} \, (^{\circ}\text{C}) \in [700\text{–}750]; \quad \lambda \in [5\text{–}9] \tag{31}$$

The curve fitting of the reference data-set yielded the following relationship:

$$\begin{aligned} V_{SOFC} = {} & 33.76 - 0.93\lambda + 1.07 \times 10^{-3}\lambda^2 - 0.28J^2 \\ & - 5.45 \times 10^{-2}T_{out} + 2.23 \times 10^{-5}T_{out}^2 + 8.33 \\ & \times 10^{-4}\lambda T_{out} - 5.15 \times 10^{-4}JT_{out} \end{aligned} \tag{32}$$

in which quadratic and cross-terms appear, thus making the dynamic Eq. (27) strongly nonlinear. In Eq. (32) T_{out} is one of the independent variables, whose values were calculated by means of the one-dimensional model. Then, they were fed as input to the identification procedure. The independent terms of
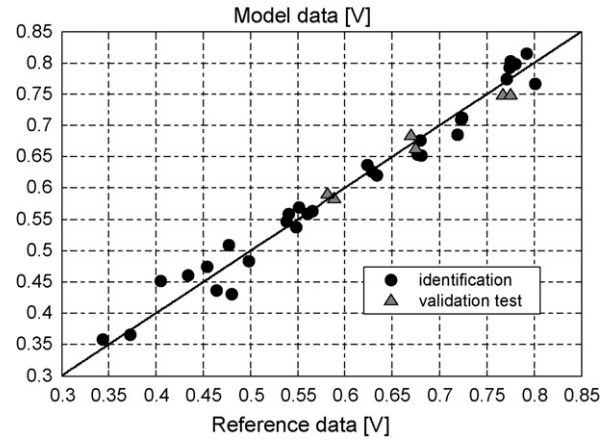

Fig. 10. Comparison between reference data and model outputs to assess the accuracy of the voltage black-box model (reformate feed, $R_2 = 0.97$, RMSE = 0.026 V).

Eq. (32) were found by means of a forward stepwise approach based on the analysis of parameters 95% confidence intervals.

The comparison between reference data and models outputs, shown in Fig. 10, demonstrates the satisfactory level of accuracy and generalization guaranteed by the voltage black-box relationship.

5.3. Analysis of SOFC transient response for stepwise load variation

The control-oriented model was tested for validation by simulating the response of V_{SOFC} to step changes in load (i.e. $\bar{J}$). Such responses were then analyzed with respect to the following performance metrics derived from literatures [15,28]:

- $V_{drop} = V_{SOFC}(t_\infty) - V_{SOFC,min}$: voltage undershoot intensity (mV);
- $\Delta V = V_{SOFC}(t_\infty) - V_{SOFC}(t_0)$: voltage difference between second and first stationary point (mV);
- τ_V: voltage relaxation time (s).

Voltage relaxation time, which is very significant for optimal balance of plant and control of SOFC systems [28], is defined as the time needed for V_{SOFC} to recover 90% of the voltage drop occurring after load or excess air step variation [15]:

$$V_{rec} = 0.9V_{drop} + V_{SOFC,min} \tag{33}$$

$$\tau_V = t|_{V_{SOFC} = V_{rec}} - t_0 \tag{34}$$

The sensitivity of performance metrics to operating conditions was also investigated and reported.

The lack of experimental transient data entailed performing qualitative validation of the model. Therefore, the results presented in the following are discussed and compared with simulations performed by Achenbach [15], who developed a three-dimensional time-dependent model for simulating the transient behavior of planar SOFC excited by load variations. Finally, a potential application of the control-oriented model

Table 3
Stepwise load variations simulated in the response to load change analysis

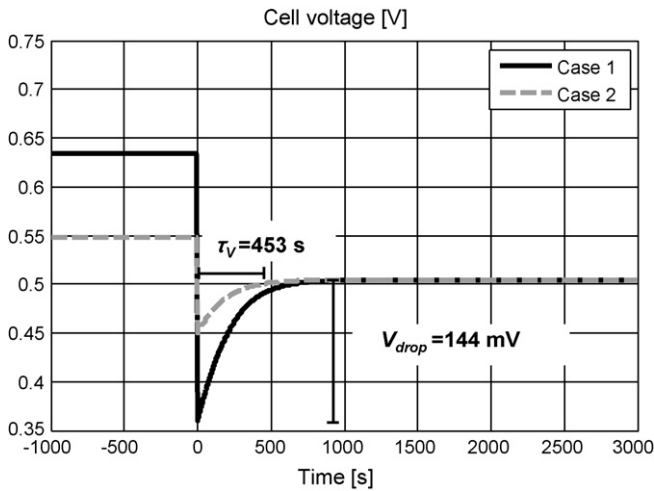| Case	$\bar{J}_0$ (A cm^{-2})	$\bar{J}_\infty$ (A cm^{-2})
1	0.4	0.7
2	0.6	0.7
3	0.4	0.5

Fig. 11. Simulated voltage response after case 1 and case 2 load steps.

is given, namely the development of a PI controller to limit temperature rise across the cell within a tolerable threshold.

5.3.1. Simulation of load stepwise variation

The SOFC response to load change was investigated for three different step variations listed in Table 3. The other inputs (i.e. λ and T_{in}) were set to their respective nominal values: 7 and 750 °C. Simulations were run by implementing the lumped model described by Eq. (27) in the Matlab-Simulink® environment. A 6.2×10^{-4} computational to real-time ratio was achieved on a PC Pentium 4 3.2 GHz, thus guaranteeing a computational burden compatible with the objectives of this paper.
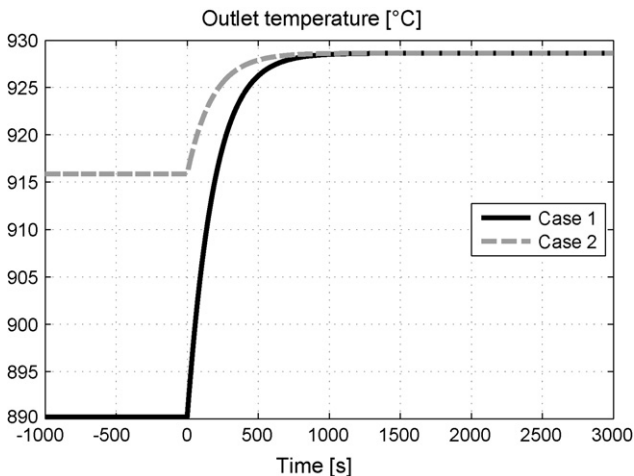

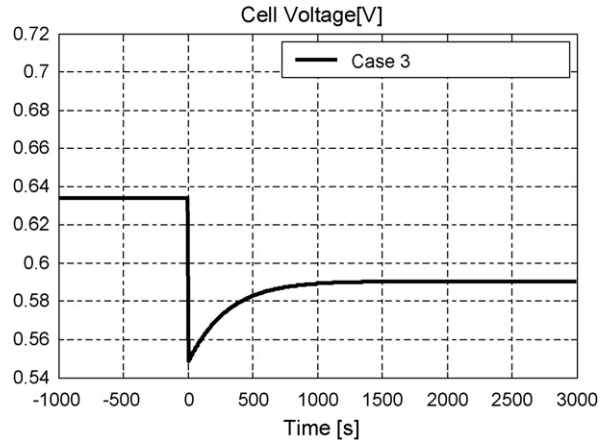Fig. 12. Simulated temperature response after case 1 and case 2 load steps.

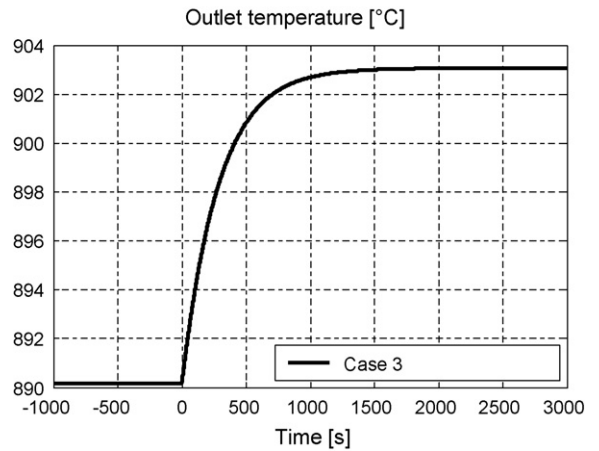Fig. 13. Simulated voltage response after case 3 load step.

Fig. 14. Simulated temperature response after case 3 load step.

Figs. 11–14 show V_{SOFC} and T_{out} responses for a methane reformate feed. For all the cases simulated, load increase causes the polarization losses to sudden increase as well, resulting in an undershoot-type response of the voltage, as shown in Figs. 11 and 13. Then, due to the slow temperature increase shown in Figs. 12 and 14, polarization losses decrease, thus allowing for a slow voltage recovery. Table 4 summarizes the results obtained by simulating cases 1–3.

The values of τ_V and τ_T indicate that thermal dynamics is significantly slow, of the order of hundreds of seconds, achieving satisfactory accordance with the simulations performed in [15,29]. As expected, since voltage dynamics is directly dependent on thermal dynamics, τ_V and τ_T are always comparable, as shown in Table 4 and in all the figures from Figs. 11 to 14.

Table 4
Performance metrics estimated for the three stepwise load transients

Case	τ_V (s)	τ_T (s)	V_{drop} (mV)
1	453	420	144
2	418	408	55
3	679	657	42

Therefore, only the dependence of τ_V on load step characteristics is deeply analyzed in the following. Voltage relaxation time tends to reduce as $\bar{J}_\infty$ increases. This behavior depends on the value of final current density reached after load step. In fact, the higher $\bar{J}_\infty$ is, the more heat is released by the electrochemical reaction, resulting in higher temperature increase, as it emerges comparing Figs. 12–14. Such an effect allows for faster compensation of polarization losses due to load increase, which in turn results in shorter τ_V for case 1 and case 2 as compared to case 3.

The values of voltage drop, listed in Table 4, indicate a significant dependence of such variable on both magnitude of load step (i.e. $\Delta\bar{J} = \bar{J}_\infty - \bar{J}_0$) and final current density (i.e. $\bar{J}_\infty$). This can be explained considering that if $\bar{J}_\infty$ is a few percent bigger than $\bar{J}_0$ (i.e. small $\Delta\bar{J}$ in cases 2 and 3), steady V_{SOFC} and T_{out} variations are not so significant, thus resulting in small V_{drop} (of the order of tens of mV, as shown in Figs. 11 and 13). Moreover, the higher $\bar{J}_\infty$ the more is the difference between voltage values at different temperature, as shown in Fig. 4. Thus, since in the first seconds after the load step T_{out} remains still closer to T_0 than T_∞, the voltage drop tends to increase with $\bar{J}_\infty$ increase.

In order to further investigate the influence on performance metrics of initial (i.e. at t_0) and final (i.e. at t_∞) step conditions, two sensitivity analysis were performed. Sensitivity of function A to variable B was evaluated as

$$S_B^A = \frac{dA}{A} \frac{B}{dB} \tag{35}$$

Fig. 15 shows the variations of V_{drop} as function of $\Delta\bar{J}$ and $\bar{J}_\infty$ with the corresponding average sensitivities (i.e. $\bar{S}_{\Delta\bar{J}}^{V_{drop}}$ and $\bar{S}_{J_\infty}^{V_{drop}}$). The figure indicates that either an increase in load step or in final current density causes the voltage drop to increase. On the other hand Fig. 16, which shows the dependence of τ_v on $\Delta\bar{J}$ and $\bar{J}_\infty$, indicates that $\Delta\bar{J}$ has not such a significant effect on relaxation time (i.e. $\bar{S}_{\Delta\bar{J}}^{\tau}$ close to 0) while, as expected, sensitivity to $\bar{J}_\infty$ (i.e. $\bar{S}_{\Delta J}^{V_{drop}}$) is negative.
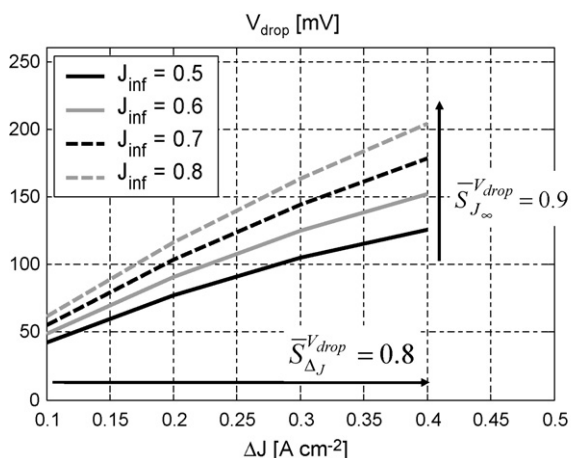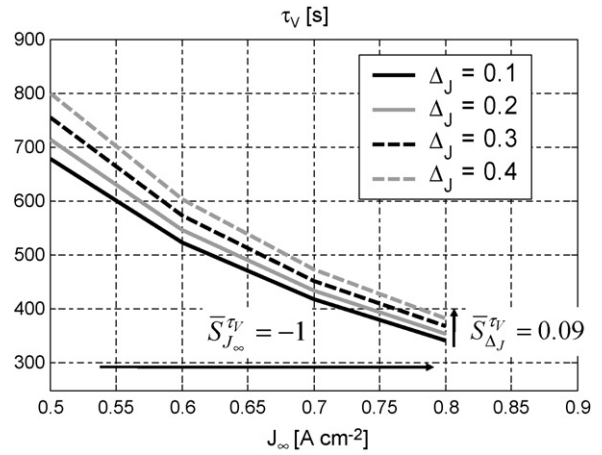

Fig. 16. Variation of τ_V as function of and corresponding average sensitivities.

5.4. Application of the control oriented model: PI controller development

SOFC power is controlled by varying the current drawn from the stack until the power demand is met. Nevertheless, the dynamics associated with load variation is characterized by two significant phenomena: voltage undershoot, described in Fig. 11; temperature increase following load increase, due to the higher heat produced via electrochemical reaction at the anode (see Fig. 12). The latter phenomenon is of particular concern, due to the thermal stresses imposed on the cell material by temperature variation. Previous studies [10,30,31] indicated that temperature variation across the cell should not overcome 100–150 °C to ensure cell components integrity.

Using the control-oriented simulator developed in the previous section, a PI controller was designed to keep temperature variation (i.e. $\Delta T = T_{out} - T_{in}$) below a safety-threshold, here set to 150 °C. To accomplish this task, the variable to be managed is the excess air λ [31]. Such control can be performed acting on the drive motor of the air supply system. For a generic fuel cell system, air can be fed by either a compressor or a blower, depending upon operating pressure requirements. Since the time constant of air supply system is much lower than temperature dynamics, hardware implementation of excess-air control can be easily accomplished. It is also worth pointing out that temperature control in an SOFC system requires to take into deep account the mutual interaction between stack and its main auxiliaries, not only air compressor/blower but reformer and heat exchangers as well. Specifically in this section, the interest is mainly devoted to assess the potentialities offered by the presented modeling methodology to address the aspects related to the SOFC component control within the entire system.

The controller design was performed referring to the SOFC modeled through Eq. (27). Reformate fuel feed was assumed. Fig. 17 sketches the control scheme adopted.

The PI was developed by tuning the proportional and integral gains until acceptable control performances in terms of system response and stability were reached. This process resulted in the

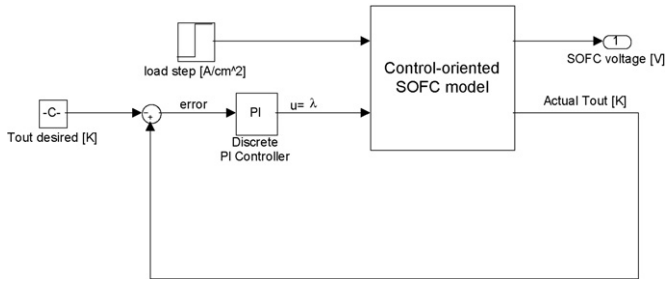Fig. 15. Variation of Vdrop as function of and corresponding average sensitivities.

Fig. 17. Diagram block of the control architecture implemented.

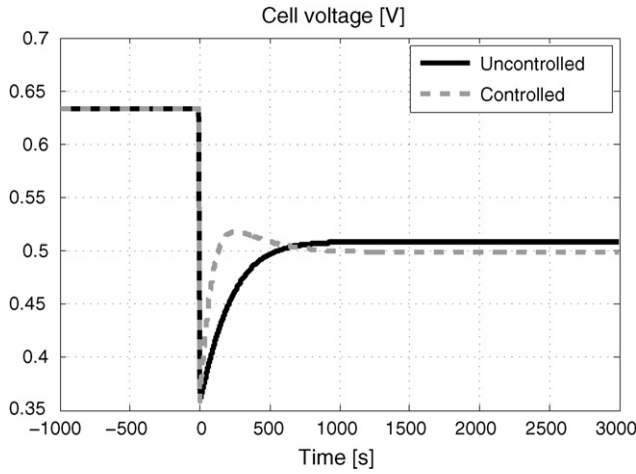
Fig. 18. Comparison between VSOFC responses in controlled and uncontrolled operation.

following gains:

$$k_p = 0.1$$
$$k_i = 5 \times 10^{-4} \quad (36)$$

Figs. 18 and 19 show the voltage and ΔT responses to load change (i.e. from $\bar{J}_0 = 0.4$ to $\bar{J}_\infty = 0.7 \, (\text{A cm}^{-2})$) for both controlled and uncontrolled SOFC operation. Fig. 19 evidences how the PI controller is capable to limit ΔT increase down
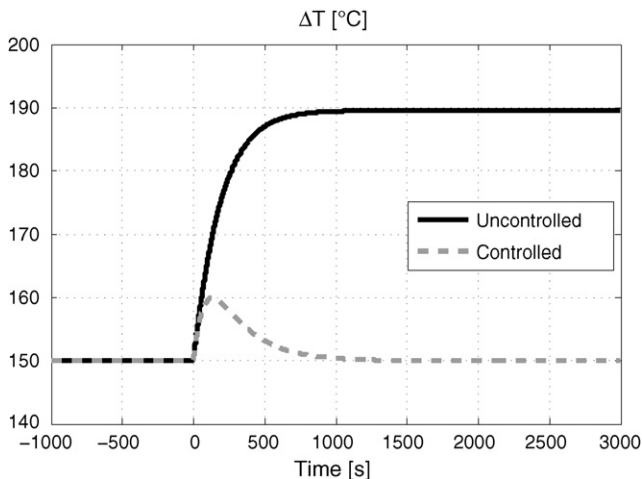

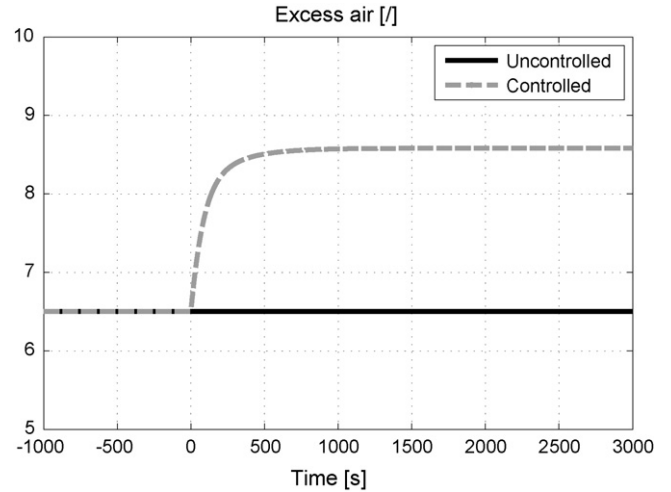Fig. 19. Comparison between ΔT responses in controlled and uncontrolled operation.

Fig. 20. Excess of air in controlled and uncontrolled operation.

to $8°$ for about 600 s before bringing ΔT back to the optimal threshold. The comparison of controlled and uncontrolled voltage responses, shown in Fig. 18, indicates that the PI action results in faster voltage drop recovery (about 100 s against 450 s). Moreover, as the safety threshold is reduced, the final voltage decreases from 0.51 to 0.5. Therefore, controlled operation can satisfactorily prevent SOFC components from thermal-stress caused damages, while slightly decreasing performance. Fig. 20 shows the λ trajectory for the controlled and uncontrolled systems. As expected, change in current load required increasing excess air to meet the safety threshold imposed on ΔT.

6. Conclusions

A hierarchical modeling approach was presented that describes solid oxide fuel cell behavior in both steady and transient conditions. A one-dimensional model for steady-state computations was developed combining a phenomenological electrochemical model with appropriate forms of the conservation equations. Its principal aim is to provide accurate estimate of the spatial variation of the main SOFC operating variables. Validation of the model was successfully performed by referring to previously published information.

Then, based on simplifying assumptions derived from literature and performance data provided by the 1D model in a hierarchical way, a control-oriented model was developed to simulate SOFC response to changes in operating conditions. Particularly, SOFC dynamics was modeled applying the conservation of energy principle to a lumped open volume that includes solid trilayer and interconnect, both made of ceramic materials. The effect of thermal dynamics was thus considered dominant with respect to mass and electrochemistry. The influence of outlet temperature variation on cell voltage was taken into account by means of a black-box relationship, identified versus reference data generated by the one-dimensional model.

The control-oriented model was tested through extensive simulations of voltage and temperature responses to changes in current load. The results showed the ability of such model in well

capturing the undershoot-type voltage response to positive load variation, thus proving the validity of the approach proposed.

SOFC dynamics was analyzed with respect to some significant performance metrics, such as voltage drop (i.e. undershoot) and voltage relaxation time. Two sensitivity analyses were carried out to evaluate the dependence of voltage drop and relaxation time on magnitude of load step and final current density. It was shown that both variables have an appreciable influence on voltage drop. Regarding relaxation time, the results indicate that it is quite sensitive to final current density value, while being substantially independent of magnitude of load step. These observations are in accordance with previous theoretical studies based on physical time-consuming approaches. Therefore, the model presented allows for significant reduction in computational burden, while guaranteeing satisfactory accuracy.

Finally, an application example of the control oriented model was reported, namely the development of a PI controller to limit temperature rise from cell inlet to outlet. The use of such controller allows reducing voltage relaxation time, while bounding in a safe range the temperature rise subsequent to a load step. Moreover, the comparison between controlled and uncontrolled system indicates the need of solving the trade-off between safe operation of cell components and cell performance, with the latter being lowered by temperature rise control.

The hierarchical approach proposed in this work can be easily extended to other cell configurations, such as low temperature and intermediate temperature anode supported cell, to develop control-oriented models suitable for (i) implementation in system-level simulators for balance of plant and system sizing calculations, such as large-scale design of automotive APUs; (ii) optimal selection of cell materials as function of desired and/or admissible current and temperature variations; (iii) off-line development of optimal energy-management strategies for automotive APUs; (iv) on-board implementation for model-based control applications.

Future work will concentrate on the development of a comprehensive simulator of reformate-fed SOFC-APUs hybridized with appropriate energy storage devices.

Acknowledgements

References

[1] T.C. Voigt, SECA: The Challenge for Small-Scale, Ultra-Low Cost SOFC Power Systems presentation held at Third Annual SECA Workshop (Solid State Energy Conversion Alliance), March 2002, Washington, DC, 2002.

[2] S.C. Singhal, Solid State Ionics 152/153 (2002) 405–410.

[3] Topsoe, Wärtsilä and Topsoe Start Co-operation in Fuel Cell Development, news appeared on topsoe website (www.topsoe.com), October 16, 2002.

[4] FELICITAS, 2002. Fuel cell power-trains and clustering in heavy-duty transport, available at http://www.felicitas-fuel-cells.info/.

[5] J. Zizelman, S. Shaffer, S. Mukerjee, 2002. Solid Oxide Fuel Cell Auxiliary Power Unit—A Development Update, SAE Paper 2002-01-0411.

[6] P. Aguiar, C.S. Adjiman, N.P. Brandon, J. Power Sources 138 (2004) 120–136.

[7] I. Arsie, M. Gambino, C. Pianese, G. Rizzo, Development and validation of hierarchical models for the design of engine control strategies, Meccanica 32 (5) (1997) 397–408.

[8] J.J. Botti, M.J. Grieve, J.A. MacBain, 2005. Electric Vehicle Range Extension Using an SOFC APU, SAE Paper 2005-01-1172.

[9] J.L. Broge, 2002. Delphi fuel-cell APU for BMW, SAE technical briefs, available at http://www.sae.org/automag/techbriefs/04-2002/page2.htm.

[10] R. Braun, 2002. Optimal Design and Operation of Solid Oxide Fuel Cell Systems for Small-Scale Stationary Applications. Doctoral dissertation, University of Wisconsin, Madison, USA.

[11] J.J. Botti, M.J. Grieve, C.E. Speck, in: Duret FP. (Ed.), Emissions Reduction through Hydrogen Enrichment, Which Fuels For Low CO_2 Engines?, Editions Technip, Paris, 2004.

[12] G. Rizzoni, J.R. Josephson, A. Soliman, C. Hubert, C.G. Cantemir, N. Dembski, P. Pisu, D. Mikesell, L. Serrao, J. Russell, M. Carroll, in: Proceedings of the SPIE, J. Unmanned Ground Veh. Technol. VII 5805 (2005) 1–12.

[13] I. Arsie, C. Pianese, G. Rizzo, R. Flora, G. Serra, Proceedings of the 14th IFAC World Congress, vol. P, Beijing, China, July 5–9, 1999, pp. 473–488.

[14] L.A. Chick, R.E. Williford, J.W. Stevenson, C.F. Windisch Jr., S.P. Simner, Proceedings of Fuel Cell Seminar, PNNL-SA-37014, Palm Springs, CA, November 19–21, 2002.

[15] E. Achenbach, J. Power Sources 57 (1995) 105.

[16] C. Haynes, 1999. Simulation of Tubular Solid Oxide Fuel Cell Behavior for Integration Into Gas Turbine Cycles. Ph.D. Thesis, Georgia Institute of Technology, Atlanta, GA.

[17] A.C. Burt, I.B. Celik, R.S. Gemmenb, A.V. Smirnov, J. Power Sources 126 (2004) 76–87.

[18] L.A. Chick, R.E. Williford, J.W. Stevenson, 2003. Spreadsheet Model of SOFC Electrochemical Performance, SECA Modeling & Simulation Training Session August 2003 (web-page: www.netl.doe.gov/publications/proceedings/03/seca-model/seca-model03.html).

[19] M. Sorrentino, A.Y. Mandourah, T.F. Petersen, Y.G. Guezennec, M.J. Moran, G. Rizzoni, Proceedings 2004 ASME IMECE, Anaheim, CA, USA, November 13–19, 2004.

[20] Fuel Cell Handbook, 6th ed., U.S. Department of Energy/National Energy Technology Laboratory Strategic Center for Natural Gas, Morgantown, WV/Pittsburgh, PA/Tulsa, OK, 2002, November.

[21] K. Keegan, M. Khaleel, L.A. Chick, K. Recknagle, S. Simner, J. Deibler, 2002. Analysis of a Planar Solid Oxide Fuel Cell Based Automotive Auxiliary Power Unit, SAE Technical Paper Series No. 2002-01-0413.

[22] S.C. Singhal, K. Kendall (Eds.), Solid Oxide Fuel Cells—Fundamentals, Design and Applications, Elsevier Ltd., Oxford, 2003, pp. 233–237.

[23] J. Larminie, A. Dicks, Fuel Cell Systems Explained, John Wiley and Sons, Chichester, West Sussex, England, 2003, pp. 1–24, 207–227.

[24] E. Achenbach, E. Riensche, J. Power Sources 52 (1994) 283–288.

[25] A.F. Massardo, F. Lubelli, J. Eng. Gas Turb. Power 122 (2000) 27–35.

[26] M. Iwata, T. Hikosaka, M. Morita, T. Iwanari, K. Ito, K. Onda, Y. Esaki, Y. Sakaki, S. Nagata, Solid State Ionics 132 (2000) 297–308.

[27] K. Sedghisigarchi, A. Feliachi, IEEE Trans. Energy Conv. 19 (2) (2004) 423–428.

[28] A. Selimovic, M. Kemm, T. Torisson, M. Assadi, J. Power Sources 145 (2005) 463–469.

[29] D. Larrain, 2005, Solid Oxide Fuel Cell Stack Simulation and Optimization, Including Experimental Validation and Transient Behavior. Ph.D. Thesis, École Polytechnique Fédérale de Lausanne, France.

[30] P. Ioraa, P. Aguiar, C.S. Adjiman, N.P. Brandon, Chem. Eng. Sci. 60 (2005) 2963–2975.

[31] P. Aguiar, C.S. Adjiman, N.P. Brandon, J. Power Sources 147 (2005) 136–147.